Amorphous Zr-based thin films fabricated by magnetron sputtering for potential application in hydrogen purification

Nayebossadri, Shahrouz; Smith, Daniel; Speight, John; Book, David

DOI:
10.1016/j.jallcom.2015.01.230

Amorphous Zr-based thin films fabricated by magnetron sputtering for potential application in hydrogen purification

Shahrouz Nayebossadri, Daniel Smith, John Speight, David Book

PII: S0925-8388(15)00328-X
DOI: http://dx.doi.org/10.1016/j.jallcom.2015.01.230
Reference: JALCOM 33294

To appear in: *Journal of Alloys and Compounds*

Please cite this article as: S. Nayebossadri, D. Smith, J. Speight, D. Book, Amorphous Zr-based thin films fabricated by magnetron sputtering for potential application in hydrogen purification, *Journal of Alloys and Compounds* (2015), doi: http://dx.doi.org/10.1016/j.jallcom.2015.01.230

Amorphous Zr-based thin films fabricated by magnetron sputtering for potential application in hydrogen purification

Shahrouz Nayebossadri*, Daniel Smith, John Speight, David Book
School of Metallurgy and Materials, University of Birmingham,
Edgbaston, Birmingham, B15 2TT, UK
E-mail: s.nayebossadri@bham.ac.uk
Tel: (+44) (0) 121 414 5213

Abstract

Amorphous hydrogen separation membranes are under development because of their resistance to hydrogen embrittlement, improved mechanical properties, resistance to corrosion and most importantly lower intrinsic cost. The Closed Field Unbalanced Magnetron Sputter Ion Plating (CFUBMSIP) is a versatile technique for deposition of high quality thin-films of almost any composition, while enabling the control of film size, thickness and shape. In this work, it was demonstrated that thin-films (~ 3-6 microns) of amorphous $Zr_{40.5}Ni_{59.5}$, $Zr_{54}Cu_{46}$ and $Zr_{30}Cu_{57.5}Y_{12.5}$ could be deposited onto glass substrates by the CFUBMSIP technique. XRD measurements only showed one broad peak for each alloy, with a peak centred between 36 and 42° 2θ, indicating that the films were amorphous. Surface analysis by SEM and confocal microscopy suggest deposition of continuous films. The thermal stability of the films appears to be mainly governed by the alloying elements and their compositions. However, the measured activation energies indicated that the nucleation and growth mechanism in the magnetron sputtered films may be different from that reported for melt-spun amorphous alloys with similar compositions.

***Keywords*:** *Hydrogen Purification, metallic membranes, amorphous alloys, thin films, Zr-based alloys, magnetron sputtering*

1- Introduction

Palladium and Pd alloy membranes are currently used for hydrogen purification [1]. However, the cost of Pd membranes is considered to be prohibitively expensive for large–scale hydrogen purification applications [2]. The cost of Pd membranes in combination with their susceptibility to hydrogen embrittlement [3] and susceptibility to surface poisoning by impurity gases such as CO_2, CO and H_2S [4,5] has motivated the investigation of alternative materials for hydrogen separation membranes. The use of amorphous materials for hydrogen separation membrane can address several problems associated with the use of crystalline materials such as hydrogen embrittlement and high cost [6]. Some of the amorphous zirconium-based membranes, and in particular $Zr_{36}Ni_{64}$, $Zr_{54}Cu_{46}$, and $Zr_{30}Cu_{60}Y_{10}$ alloys, have been shown by computational [7,8] and experimental studies [9,10] to have hydrogen permeability values close to that of Pd.

Amorphous metal membranes can be produced by melt spinning, whereby molten metal is rapidly quenched onto a spinning copper wheel resulting in a metal ribbon in which non-equilibrium microstructures can effectively be captured [11]. Numerous examples of amorphous ribbons, such as $Zr_{54}Cu_{46}$ (30–40 μm thickness) [12] and ternary Ni-Nb-Zr films [13,14] were fabricated by melt spinning for hydrogen separation membranes. However, this technique imposes certain restrictions on possible alloy compositions, as incorporation of higher melting point elements may exceed the upper temperature limit that can be experimentally achieved [8]. In addition, precise control of the shape and size of the melt spun ribbons is difficult. Maintaining a uniform ribbon thickness with desired materials properties depend on the strict control of the process parameters, such as flow of molten metal and solidification rate [15]. The morphology of the output ribbon also strongly depends on the ribbon solidification time [15].

Alternatively, a physical vapour deposition (PVD) method can be used, as reported for the fabrication of amorphous Zr–Ni [16] and Zr–Cu [17,18] thin films. PVD techniques, such as magnetron sputtering, may allow the rapid and convenient production of an amorphous membrane over a wider compositional range (compared to melt spinning), while enabling good control of the film size, shape, and thickness. The Closed Field Unbalanced Magnetron Sputter Ion Plating (CFUBMSIP) uses a high density of low energy bombarding ions for production of very dense films with relatively low internal stresses [19]. In addition, the use of low bias voltage on the work piece allows the deposition of films at a low temperature, which could be beneficial when attempting to produce amorphous alloys. This work will investigate the possibility of using this particular type of magnetron sputtering, (CFUMSIP) [19], to fabricate thin amorphous films of $Zr_{36}Ni_{64}$, $Zr_{54}Cu_{46}$, and $Zr_{30}Cu_{60}Y_{10}$ alloys, due to their comparable hydrogen permeability to Pd [7,8,9,10]. Structure, composition, surface morphology and thermal stability of the alloys will be assessed.

2- Materials and method

Zirconium, copper, nickel and yttrium sputtering targets (99.9 % purity) were obtained from Teer Coatings Ltd. Films with varying thicknesses were deposited onto 76 × 26 mm glass microscope slides (Thermo Scientific) by the Closed Field Unbalanced Magnetron Sputter Ion Plating (UPD 350-4), and were then peeled off, as shown in Figure 1.(These films would require support in order to be used as hydrogen separation membranes.) The optimum sputtering conditions to produce the desired $Zr_{36}Ni_{64}$, $Zr_{54}Cu_{46}$ and $Zr_{30}Cu_{60}Y_{10}$ amorphous films, were obtained via a series of 10 minute test coatings in which the Zr target current was varied, and the other sputtering parameters were fixed. The final sputtering conditions for each film deposition is given in Table 1. Relatively low target currents were selected, which seemed to be necessary to avoid crystallisation. The sputtering chamber was evacuated to

approximately 10^{-6} mbar prior to the depositions and refilled to ~ 2.5×10^{-3} mbar with continuous flow (25 ml/min) of ultra–high purity argon during the deposition runs. A bias voltage of 50 volts was applied to each magnetron during deposition runs. Final samples were deposited using pulsed DC, with a constant target to substrate distance and a sample rotation speed of 5 rpm, for approximately 3 h (18 runs of 10 minutes each). The cooling period between each run was designed to avoid sample overheating and possible crystallisation during the deposition process.

X-Ray Diffraction (XRD) measurements of the films were performed using a Bruker D8-Advanced diffractometer with monochromatic CuKα radiation (λ = 1.54056 Å). The surface morphology and atomic compositions were analysed by a Joel 6060 Scanning Electron Microscope (SEM) equipped with an INCA 300 Energy Dispersive Spectrometer (EDS). The surface roughness and films thicknesses were examined using an Olympus LEXT OLS 3100 mounted on a TableStable anti-vibration mounting. The system uses a 408 nm Class II ultraviolet laser source and has a planar resolution (X and Y) of 120 nm and a spatial pattern (Z resolution) of 10 nm. A part of the glass substrate was masked by Kapton tape, which was removed after the deposition, allowing step height film measurements.

Differential Scanning Calorimetry (DSC) measurements were performed on films that had been peeled-off of their glass substrates, under 3 bar Ar (flowing at 100 ml min^{-1}) using a Netzsch DSC204HP system at heating rates of 2, 5, 10, 15, and 20 °C min^{-1}.

3- Results and discussion

3.1 Structural and compositional characterisation

The X-ray diffraction patterns of Zr-based alloys after deposition are given in Figure 2. Zr–Ni, and Zr–Cu–Y alloys show common characteristic of amorphous materials with a broad XRD peak between 30–50º. A similar broad peak can be also observed for the Zr–Cu

alloy, with splits in the peak possibly suggesting some phase segregation or the formation of a small amount of nano-crystalline phase (Figure 1b). Similarly, broad XRD peaks at around 2θ = 40º were also observed for $Zr_{36}Ni_{64}$ and $Zr_{54}Cu_{46}$ alloys fabricated by melt spinning [12,9]. Hence, the XRD patterns in Figure 1 indicate that it is possible to fabricate amorphous and nano–crystalline thin–film membranes of Zr–Ni, Zr–Cu, and Zr–Cu–Y by magnetron sputtering once deposition conditions are accurately defined to avoid crystallisation.

Atomic compositions of the samples were analysed by EDS, averaging various (at least three readings) area scans (>100 μm^2) and the results are listed in Table 1. The compositions obtained by the EDS analyses are close to the intended compositions, although further optimisations in the deposition conditions may be required to achieve the target composition particularly for the Zr–Ni alloy. The fabrication of amorphous Zr–Ni alloys (with varying compositions) by magnetron sputtering was previously reported by Coulter and Driscoll [16]. EDS analysis of the deposited samples (Table 1) also suggests that good control of the thin–film composition can be achieved by precise control of the alloying elements deposition rate.

3.2 Surface morphology

The surface topographies of the magnetron sputtered alloys are shown in Figure 3a–c. SEM images suggest deposition of continuous films for all the sputtered samples. A common feature, which can be observed from the SEM images, is the formation of bubble–like structures on the film surface, with diameters of 1–4 µm. This may have occurred as a result of local loss of film adhesion to the substrate and relaxation of film deposition stresses. Further analyses of the 3–D images obtained by confocal laser microscope and their respective line–profiles also confirmed the formation of the bubble–like structures. However, the line–profiles roughness increases from $Zr_{40.5}Ni_{59.5}$ to $Zr_{30}Cu_{57.5}Y_{12.5}$ alloy, which corresponds to the density of the bubble–like structures on the surface. This was also in accordance to an increase in the ease of removing the films from the substrate. Also, a few

surface pores could be observed, particularly in the $Zr_{54}Cu_{64}$ and $Zr_{30}Cu_{57.5}Y_{12.5}$ films. Nevertheless, their approximate pore depths, which are 0.7 and 0.8 micron for $Zr_{54}Cu_{64}$ and $Zr_{30}Cu_{57.5}Y_{12.5}$ films respectively, are smaller than the overall thickness of the films (Table 1). All the films were also light-tight when visually inspected against a light source. However, the absence of pin-holes and the hydrogen selectivity of these films, should also be verified by applying a pressure differential across the films; this will be the subject of future work.

3.3 Thermal stability

The crystallisation behaviour of amorphous $Zr_{40.5}Ni_{59.5}$, $Zr_{54}Cu_{64}$ and $Zr_{30}Cu_{57.5}Y_{12.5}$ alloys are shown by the DSC traces in Figure 4a–c. Crystallisation involves nucleation and growth processes which can be related to the onset and peak temperatures of crystallisation, respectively [14]. The DSC data for $Zr_{40.5}Ni_{59.5}$ (Figure 3a) shows a peak temperature at 467 °C, lower than the reported crystallisation temperatures for $Zr_{36}Ni_{64}$ (around 550 ºC) [9,14]. The lower crystallisation temperature observed in the present work may be due to the internal stress in the thin film structure and an increased Zr content of this alloy, both of which have a known effect in lowering the thermal stability [14,16,20]. In addition, whilst DSC traces of melt–spun $Zr_{36}Ni_{64}$ showed a primary and secondary exothermic peak [14], the DSC for $Zr_{40.5}Ni_{59.5}$ (Figure 3a) of the present work shows a single exothermic peak which may correspond to a different crystallisation mechanism/path in the deposited and melt spun alloys. Crystallisation of $Zr_{54}Cu_{46}$ (Fig. 3b) shows a peak temperature at 462 ºC, which is comparable to the previously reported crystallisation temperatures [12,21,22]. A crystallisation peak temperature of 474 ºC was observed for $Zr_{30}Cu_{57.5}Y_{12.5}$ (Fig. 3c), somewhat higher than the 462 ºC for $Zr_{54}Cu_{46}$. In addition, all the samples show a single–step crystallisation within the studied temperature range. Density Functional Theory (DFT) calculations suggested [7] comparable hydrogen permeability values for amorphous

$Zr_{30}Cu_{60}Y_{10}$ and pure Pd at temperatures above 300 ºC. Therefore, the flexibility of the CFUMSIP technique in producing Zr–Cu–Y alloys with a wide range of compositions may make these alloys of interest for further experimental investigation as hydrogen separation membranes.

Activation energies, E_a, for amorphous–crystalline transitions can be obtained by assuming that the rate factor of transformation obeys an Arrhenius equation [21]. The Kissinger method [24] allows the activation energy to be calculated by carrying out DSC measurements at different heating rates, β and use of Eqn.1,

$$\frac{d\ln\left(\frac{\beta}{T_{max}^2}\right)}{d\left(\frac{1}{T_{max}}\right)}=-\frac{E_a}{R}$$

where T_{max} is the DSC peak temperature for growth and DSC onset temperature for nucleation (Supporting Information, Tables S1 and S2). Figure 4a–c shows activation energies for crystallisation (nucleation and growth) of the alloys studied here (also listed in Table 1). The nucleation activation energies of the $Zr_{40.5}Ni_{59.5}$ and $Zr_{54}Cu_{64}$ alloys are higher than their growth activation energies implying that the nucleation process is more difficult than the growth process. However, the reverse seems to apply in the case of $Zr_{30}Cu_{57.5}Y_{12.5}$ due to its higher growth activation energy when compared to its nucleation activation energy. In addition, activation energies for nucleation and growth of $Zr_{54}Cu_{46}$ and $Zr_{30}Cu_{57.5}Y_{12.5}$ alloys are higher than the activation energies obtained for $Zr_{40.5}Ni_{59.5}$ in Figure 4a-c.

The activation energies for nucleation and growth of $Zr_{40.5}Ni_{59.5}$ alloy in Fig. 4c are lower than the reported activation energies of nucleation (374.1 kJ/mol) and growth (373.5 kJ/mol) of the melt-spun $Zr_{36}Ni_{64}$ alloy obtained by isothermal and non-isothermal methods [14]. On the other hand, the growth activation energy of 395.5 kJ/mol for the $Zr_{54}Cu_{46}$ (Fig. 4b) is higher than the reported growth activation energy of ~ 360 kJ/mol for a melt-spun sample

calculated by the Kissinger method [21]. The difference in activation energy between the alloys fabricated by melt spinning and magnetron sputtering may originate from the different degrees of amorphicity and crystallisation mechanism in these alloys.

Also, in section 3.2, a higher density of bubble–like structure as a result of poor film–substrate adhesion and an increase in internal stress in the thin film structure for $Zr_{30}Cu_{57.5}Y_{12.5}$ was observed when compared to $Zr_{54}Cu_{64}$. A non-uniform stress distribution in the $Zr_{30}Cu_{57.5}Y_{12.5}$ alloy may provide high-energy sites that encourage nucleation. However, the comparable growth activation energies for both $Zr_{30}Cu_{57.5}Y_{12.5}$ and $Zr_{54}Cu_{64}$ may suggest that the growth mechanism in $Zr_{30}Cu_{57.5}Y_{12.5}$ is somehow influenced by Y addition. It has been suggested that thermal stability in amorphous alloys, is governed by geometrical and electronic effects [6]. For example, atomic size mismatch when Zr was partially substituted by Nb in $Zr_{36}Ni_{64}$ alloy, disrupted the alloy crystallisation path [6]. Here, incorporation of Y in the $Zr_{30}Cu_{57.5}Y_{12.5}$ increases the atomic size mismatch (atomic radius (nm): Y=0.1802, Zr=0.1603 and, Cu=0.1278). This could inhibit the long-range atomic diffusion required for $Zr_{30}Cu_{57.5}Y_{12.5}$ growth.

Although the thermal stability of these alloys appears to be mainly governed by the alloying elements and their compositions, the nucleation and growth mechanism in the magnetron sputtered thin films may be different from similar alloys fabricated by melt spinning

4- Conclusions

The feasibility of fabricating Zr–based amorphous thin–films by the CFUMSIP technique, for possible application as hydrogen separation membranes, was investigated. Structural (XRD) and compositional analysis showed that amorphous $Zr_{40.5}Ni_{59.5}$, $Zr_{54}Cu_{46}$ and $Zr_{30}Cu_{57.5}Y_{12.5}$ alloys were formed. All the films were continuous and of low pinhole density; but surface roughness was shown to be lowest in $Zr_{40.5}Ni_{59.5}$ and highest in

$Zr_{30}Cu_{57.5}Y_{12.5}$ as a result of the local loss of film– substrate adhesion and stresses. The thermal stability of $Zr_{40.5}Ni_{59.5}$ was shown to be lower than melt–spun $Zr_{36}Ni_{64}$ alloy probably because of its higher Zr content. Nevertheless, the thermal stability of $Zr_{54}Cu_{46}$ was comparable to the reported values for the melt-spun alloy with a similar composition. The difference in the reported activation energy for the alloys fabricated by melt spinning and the calculated activation energy for the alloys fabricated by (CFUMSIP) technique may be related to different degrees of amorphicity and crystallisation mechanisms. Although thermal stability appears to be relatively unaffected by the fabrication method, the nucleation and growth mechanism in the sputtered thin-films of the alloys studied here may differ from that in corresponding melt-spun alloys.

Acknowledgments

Support from the EPSRC SUPERGEN Delivery of Sustainable Hydrogen (EP/G01244X/1), the Birmingham Science City Hydrogen Energy projects, and the EPSRC Hydrogen and Fuel Cell Supergen Hub (EP/J016454/1), is gratefully acknowledged.

References

1. S. Uemiya, Brief review of steam reforming using a metal membrane reactor, Top. Catal. 29 (2004) 79-84.
2. A. Criscuoli, A. Basile, E. Drioli, O. Loiacono, An economic feasibility study for water gas shift membrane reactor, J. Membr. Sci. 181 (2001) 21-27.
3. V. Jayaraman, Y.S. Lin, Synthesis and Hydrogen Permeation Properties of Ultrathin Palladium-Silver Alloy Membranes, J. Membr. Sci. 104 (1995) 251-262.
4. A.L. Mejdell, M. Jøndahl, T.A. Peters, R. Bredesen, H.J. Venvik, Effects of CO and CO_2 on hydrogen permeation through a ~3μm Pd/Ag 23wt.% membrane employed in a microchannel membrane configuration, Sep. Purif. Technol. 68 (2009) 178-184.
5. C.H. Chen, Y.H. Ma, The effect of H_2S on the performance of Pd and Pd/Au composite membrane, J. Membr. Sci. 362 (2010) 535-544.
6. M.D. Dolan N.C. Dave, A.Y. Ilyushechkin, L.D. Morpeth, K.G. McLennan, Composition and operation of hydrogen-selective amorphous alloy membranes, J. Membr. Sci. 285 (2006) 30-55.
7. S. Hao, D.S. Sholl, Rapid prediction of hydrogen permeation through amorphous metal membranes: an efficient computational screening approach, Energy Environ. Sci. 6 (2013) 232-240.

8. S.Q. Hao, D.S. Sholl, Computational prediction of durable amorphous metal membranes for H_2 purification, J. Membr. Sci. 381 (2011) 192-196.
9. M.D. Dolan, S. Hara, N.C. Dave, K. Haraya, M. Ishitsuka, A.Y. Ilyushechkin, K. Kita, K.G. McLennan, L.D. Morpeth, M. Mukaida, Thermal stability, glass-forming ability and hydrogen permeability of amorphous $Ni_{64}Zr_{36-x}M_x$ (M = Ti, Nb, Mo, Hf, Ta, or W) membranes, Sep. Purif. Technol. 65 (2009) 298-304.
10. S. Hara, N. Hatakeyama, N. Itoh, H. –M. Kimura, A. Inoue, Hydrogen permeation through palladium-coated amorphous Zr-M-Ni (M=Ti, Hf) alloy membranes, Desalination 144 (2002) 115-120.
11. M.D. Dolan, Non-Pd BCC alloy membranes for industrial hydrogen separation, J. Membr. Sci. 362 (2010) 12-28.
12. H.R.Wang, Y.F. Ye, Z.Q. Shi, X.Y. Teng, G.H. Min, Crystallization processes in amorphous $Zr_{54}Cu_{46}$ alloy. J. Non-Cryst. Solids 311 (2002) 36-41.
13. S.N. Paglieri, N.K. Pal, M.D. Dolan, S.M. Kim, W.M. Chien, J. Lamb, D. Chandra, K.M. Hubbard, D.P. Moore, Hydrogen permeability, thermal stability and hydrogen embrittlement of Ni-Nb-Zr and Ni-Nb-Ta-Zr amorphous alloy membranes, J. Membr. Sci. 378 (2011) 42-50.
14. S.M. Kim, D. Chandra, N. K. Pal, M.D. Dolan, W. M. Chien, A. Talekar, J. Lamb, S.N. Paglierri, T. B. Flanagan, Hydrogen permeability and crystallisation kinetics in amorphous Ni-Nb-Zr alloys, Int. J. Hydrogen Energy 37 (2012) 3904-3913.
15. E.A. Theisen, M.J. David, S.J. Weinstein, P.H. Steen, Transient behavior of the palnar flow melt spinning process. Chemical Engineering Science, 65, (2010) 3299-3259.
16. K. Coulter, D. Driscoll, Amorphous alloy membranes for high temperature hydrogen, DOE hydrogen program. FY 2010 annual progress report, 86-89.
17. K. Kondoh, J. Fujita, J. Umeda, and T. Serikawa, Estimation of Compositions of Zr-Cu Binary Sputtered Film and Its Characterization, Res. Lett. Mater. Sci., vol. 2008, (2008) 1–5.
18. L. Li, D. Zhang, M. Li, and H. Wang, Amorphous phase formation of Zr–Cu thin films fabricated by magnetron co-sputtering, Mater. Sci. Polnad, vol. 27, no. 2, (2009) 539-544
19. UK Patent Number 2,258.343. Teer Coatings Ltd.
20. M. Dolan, N. Dave, L. Morpeth, R. Donelson, D. Liang, M. Kellam, S. Song, Ni-based amorphous alloy membranes for hydrogen separation at 400 °C, J. Membr. Sci. 326 (2009) 549-555.
21. Z. Altounian T. Guo-lua, J.O. Strom-Olsen, Crystallisation characteristics of CuZr metallic glasses from $Cu_{70}Zr_{30}$ to $Cu_{25}Zr_{75}$, J. Appl. Phys. 53 (1982) 4755-4760.
22. K. Dini, R.A. Dunlap, Crystallisation and hydrogen absorption in amorphous $Cu_{60}Zr_{40}$ and $Cu_{50}Zr_{50}$. J. Phys. F: Met. Phys. 15 (1985) 273-277.
23. S.Hao, D.S. Sholl, Rapid prediction of hydrogen permeation through amorphous metal membranes: an efficient computational screening approach. Energy Environ. Sci. 6 (2013) 232-240.
24. H.E. Kissinger, Variation of peak temperature with heating rate in differential thermal analysis, J. Res. Nat. Bur. Stand., 57 (1956) 217-221.

Figures

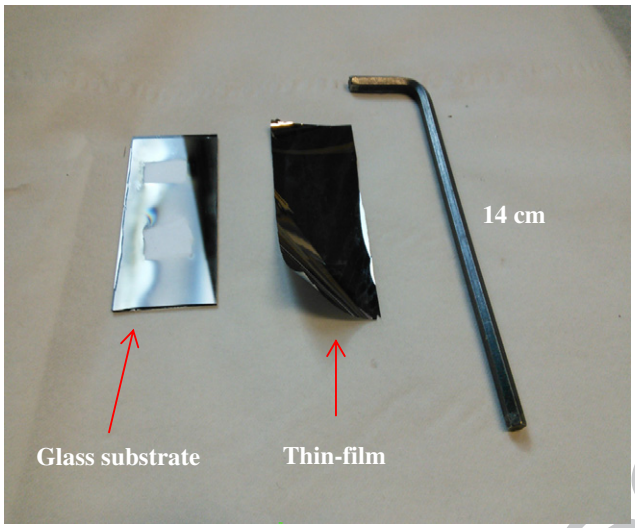

Figure1: Magnetron sputtered thin film peeled off the glass substrate.

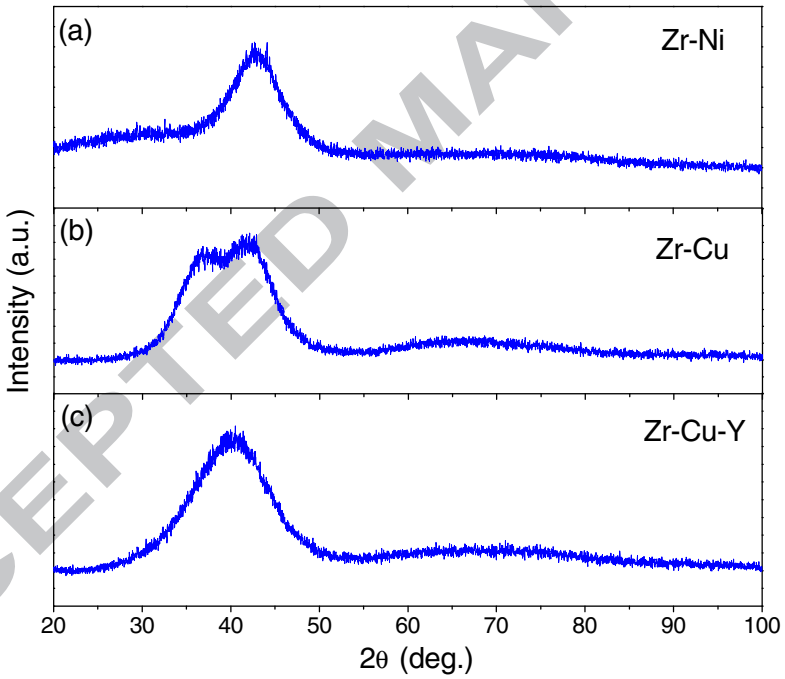

Figure 2: XRD diffraction patterns of as fabricated (a) Zr–Ni, (b) Zr–Cu (c) Zr–Cu–Y alloys by magnetron sputtering.

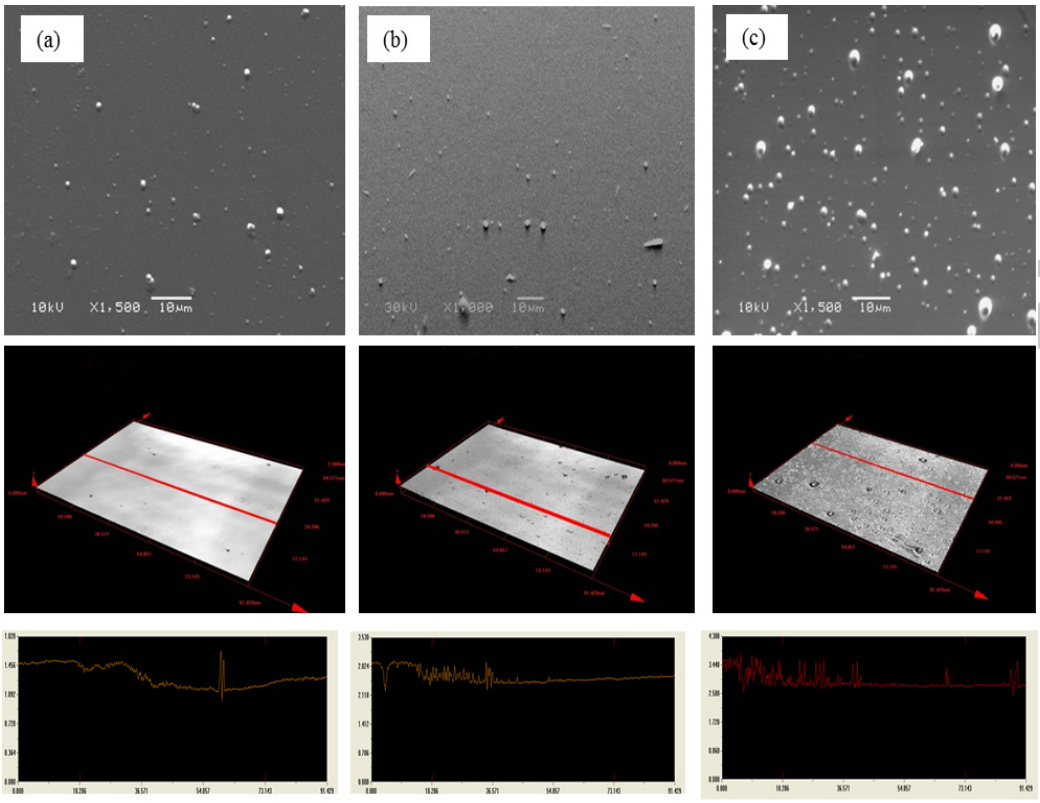

Figure 3: SEM image of the surface topography of as deposited (a) $Zr_{40.5}Ni_{59.5}$, (b) $Zr_{54}Cu_{46}$ and (c) $Zr_{30}Cu_{57.5}Y_{12.5}$ alloys. The corresponding confocal laser microscope image and line-profile for each sample is shown underneath.

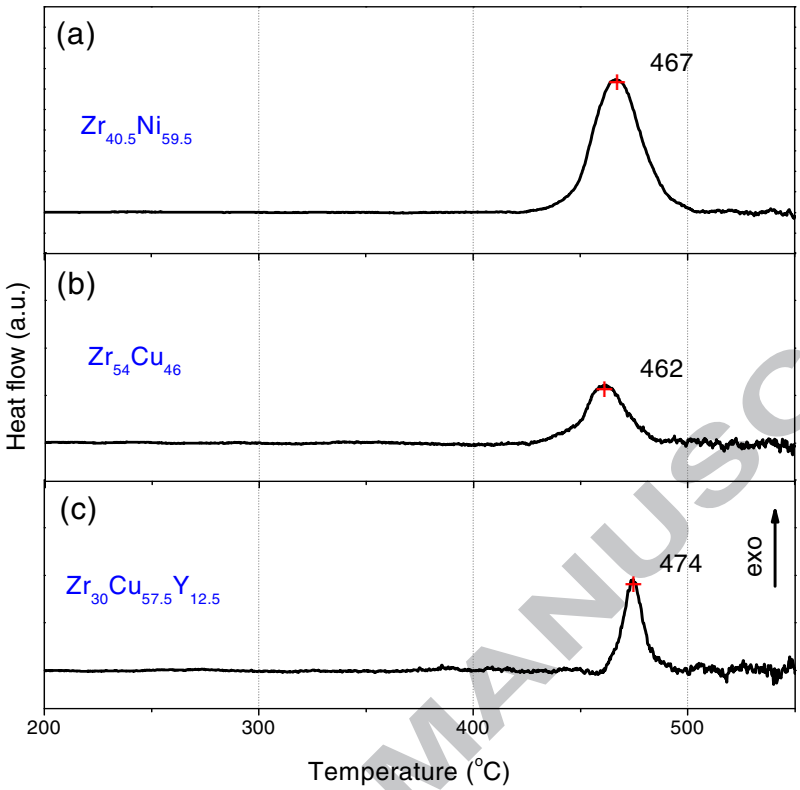

Figure 4: DSC traces for crystallisation of (a) $Zr_{40.5}Ni_{59.5}$, (b) $Zr_{54}Cu_{46}$ and (c) $Zr_{30}Cu_{57.5}Y_{12.5}$ alloys under 3 bar Ar with a heating rate of 5 ºC min^{-1}.

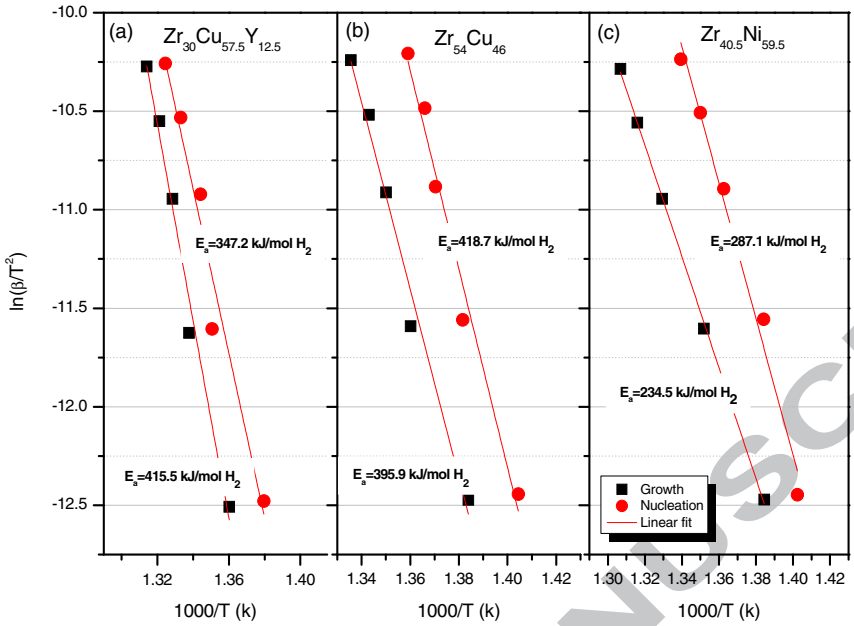

Figure 5: Activation energies for nucleation and growth of (a) $Zr_{30}Cu_{57.5}Y_{12.5}$, (b) $Zr_{54}Cu_{46}$ and (c) $Zr_{40.5}Ni_{59.5}$ alloys, using the Kissinger method with heating rates of 2, 5, 10, 15, and 20 ºC min^{-1}.

Tables

Table 1: Sputtering conditions and compositional analyses of the alloys fabricated by magnetron sputtering. The film thicknesses and the activation energies for nucleation and growth (see Fig. 5) of each sample are also listed.

alloy	Target current (A)				EDS (at.%)	Film thickness (μm)	E_a (kJ/mol)	
	Zr	Cu	Y	Ni			Nucleation	Growth
$Zr_{54}Cu_{46}$	1.42	0.5	-	-	$Zr_{54}Cu_{46}$	5.7	418.7±5.3	395.9±4.3
$Zr_{30}Cu_{60}Y_{10}$	1.25	0.8	0.5	-	$Zr_{30}Cu_{57.5}Y_{12.5}$	5.9	347.2±5.8	415.5±4.5
$Zr_{36}Ni_{64}$	0.76	-	-	0.5	$Zr_{40.5}Ni_{59.5}$	3.5	287.1±3.3	234.5±0.5

Highlights

- Thin-film (~ 3-6 microns) amorphous Zr–Ni, Zr–Cu and Zr–Cu–Y alloys for hydrogen separation membranes were successfully fabricated by the Closed Field Unbalanced Magnetron Sputter Ion Plating (CFUBMSIP) technique.
- Surface analyses showed deposition of dense and continuous films.
- Thermal stability of these alloys seems to be relatively unaffected by the fabrication method.
- The measured activation energies suggest the possibility for different nucleation and growth mechanism in the magnetron sputtered thin films when compared to the corresponding melt-spinning samples.